The Effect of Graphite Addition on Thermal Conductivity, Microstructure, and Electrochemical Impedance Spectroscopy of AlN Ceramics

Tun Wang
Shanghai University
Jianjun Xie
Shanghai University
Lei Zhang
Shanghai University
Tao Lu
Shanghai University
Maomao Ding
Shanghai University
Lingcong Fan
Shanghai University
Ding Zhou
Shanghai Institute of Technology
Ying Shi (yshi@shu.edu.cn)
Shanghai University

Research Article

Keywords: Aluminum nitride, Graphite, Grain boundary, Thermal conductivity, Impedance spectroscopy

Posted Date: October 5th, 2021

DOI: https://doi.org/10.21203/rs.3.rs-929961/v1

The Effect of Graphite Addition on Thermal Conductivity, Microstructure, and Electrochemical Impedance Spectroscopy of AlN Ceramics

Tun Wang[1], Jianjun Xie[1,*], Lei Zhang[1], Tao Lu[1], Maomao Ding[1], Lingcong Fan[1], Ding Zhou[2], Ying Shi[1,*]

1. School of Materials Science and Engineering, Shanghai University, Shanghai 200444, China

2. School of Materials Science and Engineering, Shanghai Institute of Technology, Shanghai 200235, China

Abstract: Graphite/ aluminum nitride (AlN) multiphase ceramics are pressureless sintered under 1850°C using Dy_2O_3 and CaF_2 as sintering additives. The effects of added graphite on microstructure, thermal conductivity, and electrochemical impedance spectroscopy of AlN ceramics were investigated. It was found that with 1wt% graphite addition the thermal conductivity of AlN in the through-plane to can achieve 210W/(m·K), which 25% higher than that of AlN without graphite. The graphite addition eliminates the oxygen impurity in AlN by a carbon reduction reaction in form of nanosized Dy_2O_3 particles. From electrochemical impedance spectroscopy manifested that the activation energy ($E_{a,g}$) of samples in grains is increased from 0.784 eV to 1.112 eV, suggesting that the concentrations of defects and impurities of Graphite/AlN multiphase ceramics are lower than those of monophase AlN ceramics.

Graph Abstract:

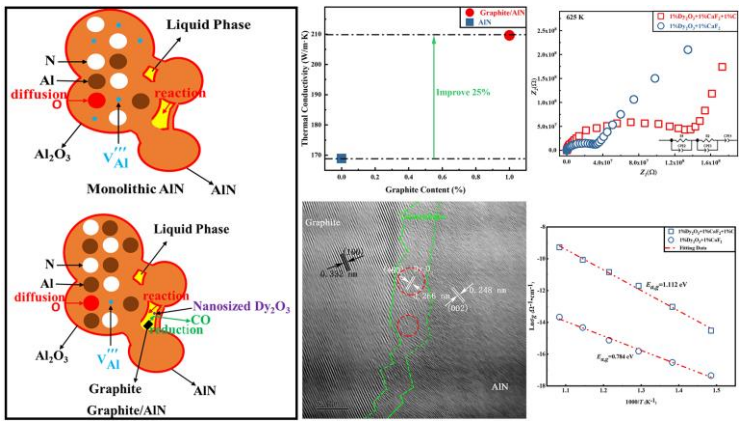

Keywords: Aluminum nitride, Graphite, Grain boundary, Thermal conductivity,

*Corresponding authors
E-mail addresses:yshi@shu.edu.cn, xiejianjun@shu.edu.cn

Impedance spectroscopy

1. Introduction

AlN ceramics are deemed to be an up-and-coming candidate for the application of high temperature structural materials in electronics devices because of high thermal conductivity, good matching of thermal expansion coefficient to that of silicon, excellent dielectric property and mechanical properties[1-5]. The thermal conductivity of AlN ceramics is closely related to the content of oxygen impurities in the powder. The effect of oxygen impurities on AlN samples was researched by Slack et al.[6-9], which could be described by the following equation:

$$Al_2O_3 \xrightarrow{AlN} 2Al_{Al} + 3O_N^{\bullet} + V_{Al}''' \quad (1)$$

The oxygen atom is incorporated into the AlN lattice to replace the N atom, forming aluminum vacancies. It has been widely recognized that phonon conduction is the thermal conduction mechanism of AlN[10-13]. The movement of phonons is influenced by the scattering of aluminum vacancies[14-16]. Therefore, the thermal conductivity of AlN samples is greatly limited by aluminum vacancies.

Doping sintering additives is considered to be an effective approaching that can fabricate high thermal conductivity AlN ceramics. Non-oxide additives, alkaline earth oxides and rare earth oxides are commonly adopted to be sintering additives for AlN ceramics[17-19]. In general, sintering additives mainly improve the thermal conductivity of AlN ceramics through two ways: During the sintering process, sintering additives can promote the densification of AlN ceramics by forming a liquid phase. Due to the reaction with sintering additives, oxygen impurities are fixed at the grain boundary as interphase newly formed[20,21]. The amount of aluminum vacancy decreases when the diffusion behavior of oxygen impurities into the AlN lattice is restrained[22,23].

Unfortunately, common sintering additives can prevent oxygen impurities from diffusing into the AlN lattice, but it does not reduce the oxygen content of the AlN ceramics. The excessive grain boundary phase might enhance the relative contact area between the grain boundary phase and the AlN grains. This situation would bring

about declining of the thermal conductivity of the AlN sample[24-26]. The secondary annealing method is often used to anneal the AlN samples for reducing the oxygen content in the AlN ceramics and eliminating the influence of the grain boundary on the thermal properties of the AlN ceramics[27-29]. Watari et al. found that the thermal conductivity of the AlN samples was effectively enhanced by heat treatment using the graphite furnace[30,31]. The reduction atmosphere was produced in the graphite furnace at a high temperature. The oxygen content and thermal conductivity of the samples were improved by the carbothermal reduction, which was further confirmed by Koji [32] et al., Kim et al.[33] and Jiang et al. [34] .

In the present work, the graphite/AlN multiphase ceramics with high thermal conductivity were fabricated by pressureless sintering with aid of Dy_2O_3, and CaF_2. The experimental results indicate that addition of graphite can reduce the oxygen content and aluminum vacancy concentration, purify the lattice and grain boundary, resulting in an obvious enhancement of thermal conductivity of the AlN sample. Moreover, the electrochemical impedance spectroscopy of the graphite/AlN multiphase ceramics were characterized to study the relevant mechanism of thermal conductivity of AlN ceramics under the condition of graphite.

2. Experimental Procedure

Commercially available AlN powders (Grand E, Tokuyama Soda Co. Ltd., Japan) containing 0.85 wt% oxygen impurities are selected as the raw material. The content of alumina was estimated at 1.81 wt%, assuming that all oxygen impurities of AlN come from alumina. The average particle size and the specific surface of the powder are 0.8 μm and 3.26 m^2/g, respectively. The morphology of AlN powder was observed in Fig. 1a. The 1 wt% Dy_2O_3 (2.93 um，99.99%, Sinopharm Chemical Reagent Co., Ltd., China) and 1 wt% CaF_2 (511.8 nm，99.99%, Sinopharm Chemical Reagent Co., Ltd., China) were blended in the samples as the binary sintering additives. Graphite powders (96.4%, Cabot Corp., America), whose average particle size is 18 nm, were mixed with the AlN powder. The microstructure of graphite was shown in Fig. 1b. The contents of graphite are 0 wt%, 0.1 wt%, 0.5 wt%, 1 wt%, 1.5 wt% and 2 wt%, as

shown Table 1. The absolute ethanol was poured into these powders and ball-milled for 12 h using the planetary ball mill (TENCAN Technology Co. Ltd., China) with alumina balls. After drying in vacuum, the mixed powders were compacted into a pellet of Φ17 mm and 5 mm thickness by uniaxially die pressing, followed by cold isostatic pressing at a pressure of 200 MPa. These samples are densified by pressureless-sintering under 1850°C for 2~24 h in the flowing nitrogen atmosphere.

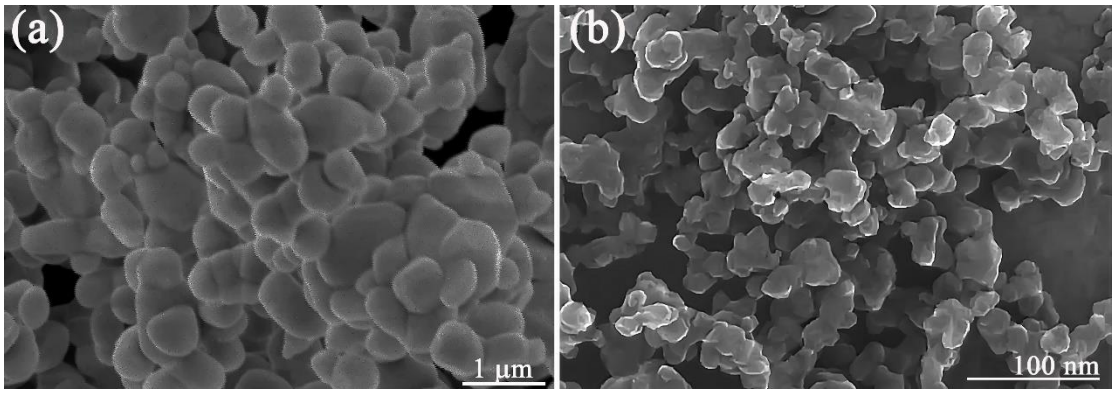

Fig. 1 The SEM micrograph of: (a) AlN powder and (b) grahite powder.

Table 1 Compositions of prepared AlN samples

Symbol	Sample composition (wt%)			
	Dy_2O_3	CaF_2	Grahpite	AlN
C_0	1	1	0	98
$C_{0.1}$	1	1	0.1	97.9
$C_{0.5}$	1	1	0.5	97.5
C_1	1	1	1	97
$C_{1.5}$	1	1	1.5	97.5
C_2	1	1	2	96

AlN ceramic discs were lapped and polished to 12.7 mm in diameter and 2 mm in thickness to measure thermal conductivity. The thermal conductivity of AlN ceramics was measured at room temperature (R.T.) using the Laser Flash Thermal Constants Analyzer (LFA-467, Netzsch, Selb, Germany). The relative densities were determined by the Archimedes method assuming that theoretical density (TD) of AlN ceramics is

3.26 $g \cdot cm^{-3}$. Crystalline phases of AlN samples were tested by X-ray diffraction analyzer (XRD, D/MAX-2200, Rigaku, Japan) with a scanning rate of $4^{\circ} min^{-1}$. The polishing surface microstructures of the AlN ceramics were observed by the scanning electron microscope (SEM, EM-30^{+}, COXEM, South Korea). The TEM samples of AlN ceramics were fabricated by the dual-beam focused ion beam microscope (FIB, Nova 600 Nanolab, FEI, USA). The high resolution structural features about grain and grain boundary micromorphology were detected by the transmission electron microscope (TEM, F20 G2, FEI tecnai, USA). The element distribution at the grain boundary was analyzed with energy dispersive X-Ray spectroscopy (EDS, Oxford Instruments X-Max^{N} 80T, Oxford, UK). Electrochemical impedance spectroscopy of the AlN sample was performed from 0.1 Hz to 1 MHz frequency range using Zahner-Elektrik IM6 workstation (Kronach, Germany) and the corresponding software Zahner Thales Z2.2.9. The testing temperature is ranged from R.T. to 700 °C.

3. Results and discussion

3.1 Phase compositions evolution of AlN/graphite ceramics

The AlN was exhaustively researched by XRD. Fig. 2 shows the XRD diffraction pattern of samples sintered at 1850°C for 2 h and 12 h. All samples have the AlN phase as the master phase. The grain boundary phase of samples sintering for 2h mainly was constituted of $Dy_3Al_5O_{12}$ (DAG phase). Sintering at 1850°C for 12h, the second phase of the graphite-free AlN sample transformed to Dy_2O_3 and $Dy_4Al_2O_9$ (DAM phase), but only the Dy_2O_3 phase existed in the graphite-doped AlN sample. During the preparation period of the AlN ceramic, the Dy_2O_3 first reacted with the Al_2O_3 layer on the AlN surface to form the DAG phase. The DAG phase gradually converted into the DAM phase during the long-term holding temperature process. Lastly, the DAM was reduced to the Dy_2O_3 phase by the graphite. The reaction equations are noticed as 3, 4, 5, and 6. All samples were sintered in a graphite resistance furnace in this experiment. Hence, some Dy_2O_3 phases are also found in the graphite-free AlN sample.

$$3Dy_2O_3+5Al_2O_3 \rightarrow 2Dy_3Al_5O_{12}(DAG) \quad (3)$$

$$Dy_3Al_5O_{12}+Dy_2O_3 \rightarrow 5DyAlO_3(DAM) \quad (4)$$

$$2DyAlO_3+Dy_2O_3 \rightarrow Dy_4Al_2O_9(DAP) \quad (5)$$

$$Dy_4Al_2O_9+3C+N_2 \rightarrow 2Dy_2O_3+2AlN+3CO\uparrow \quad (6)$$

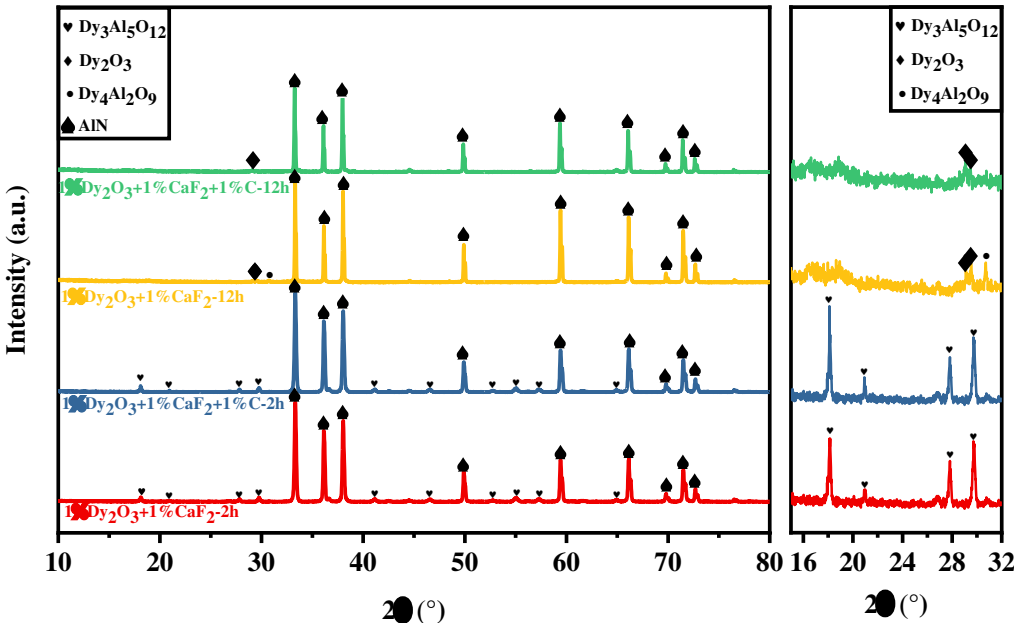

Fig. 2 XRD patterns of Graphite/AlN multpahse ceramics sintered at 1850°C.

3.2 The effect of graphite addition on the thermal conductivity of AlN ceramics

The Dy_2O_3 and CaF_2 as the sintering aids can improve the sample's thermal conductivity from Fig. 3. Our previous work has studied the specific efficacy of those sintering aids in the AlN sintering process [35]. The influence of graphite and holding time on the thermal conductivities of graphite/AlN multiphase ceramics is further explored in this work. As shown in Fig. 3, the thermal conductivity of graphite/AlN ceramics first increases and then decreases as holding time extended. The sample at sintered 12 h has the highest thermal conductivity. Besides, the thermal conductivity of samples is effectively improved by doping graphite. For example, the thermal conductivity of ceramics sintered at 1850°C for 12 h was enhanced from 169 W/(m·K) to 210 W/(m • K) when 1 wt% graphite was added in samples.

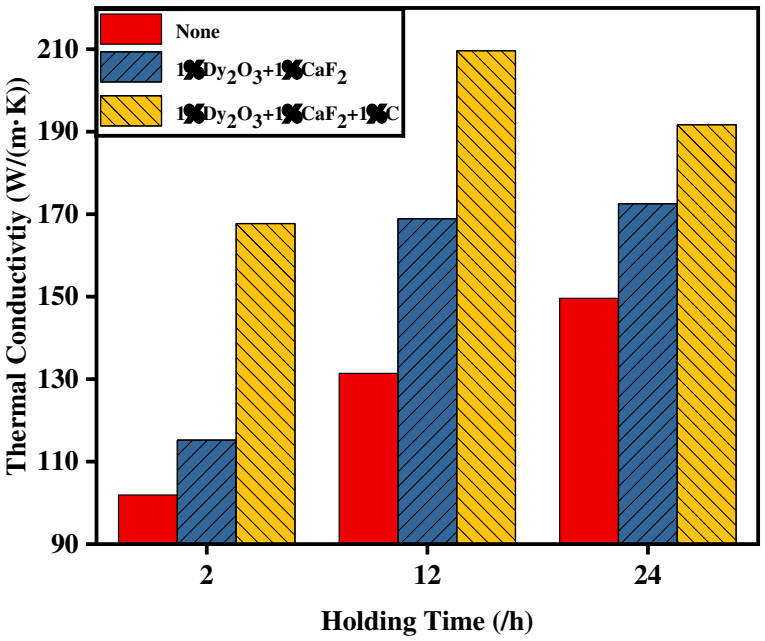

Fig. 3 The dependence of holding times on the thermal conductivity of the AlN sample with 1 wt% graphite sintered at 1850°C.

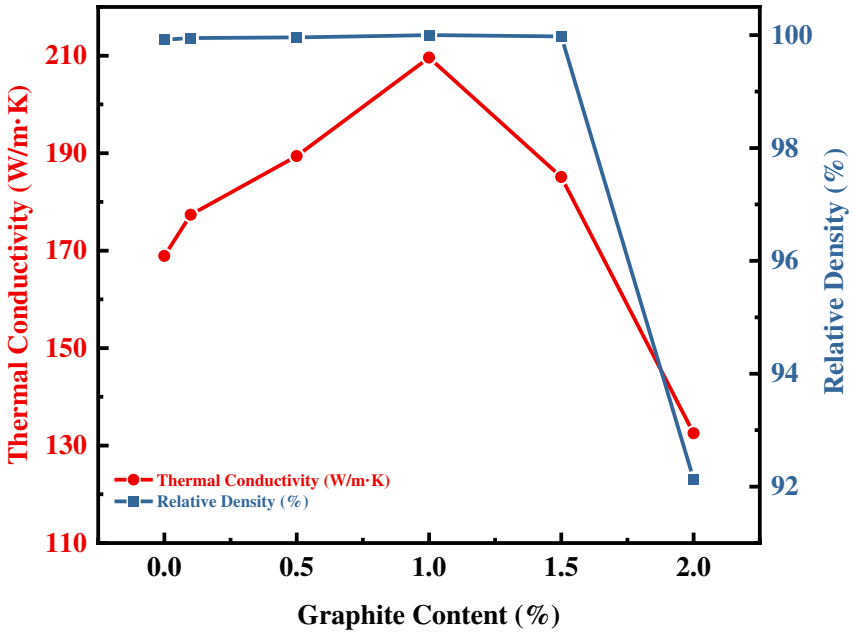

Fig. 4 The influence of graphite on thermal conductivity and relative density of AlN sample sintered at 1850°C for 12 h.

The AlN ceramics with 0 wt%, 0.1 wt%, 0.5 wt%, 1 wt%, 1.5 wt%, and 2 wt% graphite was sintered at 1850°C for 12 h. The relative density and thermal conductivity of AlN are obviously enhanced by additional excessive graphite might be constituted graphite agglomeration sintering additives. The effects of the graphite

incorporation on the density and thermal conductivity of samples are displayed in Fig. 4. It was clear that the relative densities of graphite/AlN ceramics kept almost theoretical value when the contents of graphite were less than 1.5 wt%. In contrast, it decreased drastically to 92% when graphite content attained 2.0 wt%. Meanwhile, the thermal conductivity of graphite/AlN raised to 210 W/(m·K) when graphite addition attained 1wt%, followed by a sharp decline to 125 W/(m·K) as the graphite content reached 2wt%.

3.3 The microstructure of AlN/graphite ceramics

Fig. 5a to Fig. 5f showed the microstructure of the addition of different content graphite to the sample. The sintering additives and alumina formed the second phase randomly distributed at the grain boundary in the graphite-free AlN as grain boundary phase (Fig. 5a). As known in Fig. 5b to Fig. 5d, the grain boundary phase is gradually replaced by graphite, and the grain size of the sample is reduced, with the ratio increase of graphite in the AlN ceramic. Excessive graphite forms a large number of agglomerations and pores in the AlN ceramic, causing a detrimental effect on the grain growth and ceramics densification (Fig. 5e and Fig. 5f). Therefore, the appropriate amount of graphite can eliminate the grain boundary phase and improve the thermal conductivity in the sintering process of aluminum nitride ceramics. However, graphite agglomeration is observed in the AlN ceramics with graphite content further enhanced, resulting in the sharp decrease of the thermal conductivity and relative density of AlN samples. This phenomenon is because graphite powder might be negative to the densification process of AlN because of harmfully affecting material diffusion in the AlN sintering process. The optimal content of graphite in the AlN samples was 1 wt%. The sample has the highest thermal conductivity and relative density at this time.

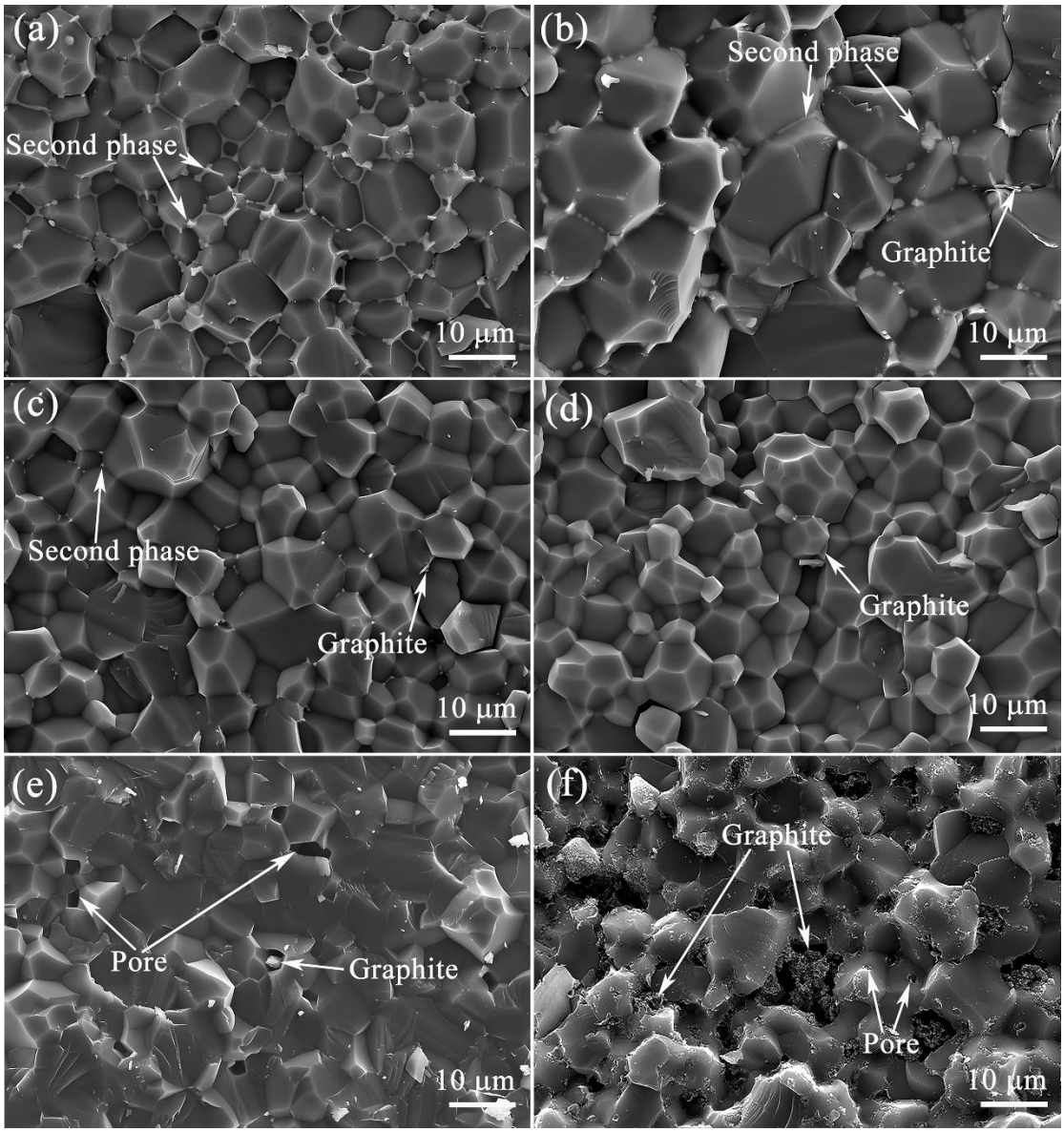

Fig. 5 The microstructure evolution of different graphite content AlN sample sintered at 1850°C for 12 h: (a) C_0; (b) $C_{0.1}$; (c) $C_{0.5}$; (d) C_1; (e) $C_{1.5}$; (f) C_2.

To further investigate the influence of graphite on the microstructure and element distribution of grain boundary, the grain boundary of AlN ceramics is characterized by TEM and EDS. Fig. 6a shows the grain boundary area containing graphite. The FIB technique fabricates the AlN HRTEM (High-resolution transmission electron microscopy) foil which is employed for the TEM test. The specific microstructure is discovered in Fig. 6b. In particular, the bright white area in Fig. 6b center is hollow, which may have been produced in the process of AlN foil fabricated using FIB. The

EDS line scan characterizes the element distribution at the grain boundary. In Fig. 6c, the element on both sides is mainly aluminum and nitride, and the element of the middle area is carbon. The detailed distribution situation about oxygen, dysprosium, and calcium elements at the grain boundary between graphite and AlN grains is observed in Fig. 6d. Little Ca element existed at the grain boundary. This result indicates that the Ca rapidly volatilizes from the AlN green body during the sintering process. Scanning from left to right along the line in Fig. 6d, the enrichment region of the O element was first observed in the grain boundary. Besides, the enriched area of the Dy element is found.

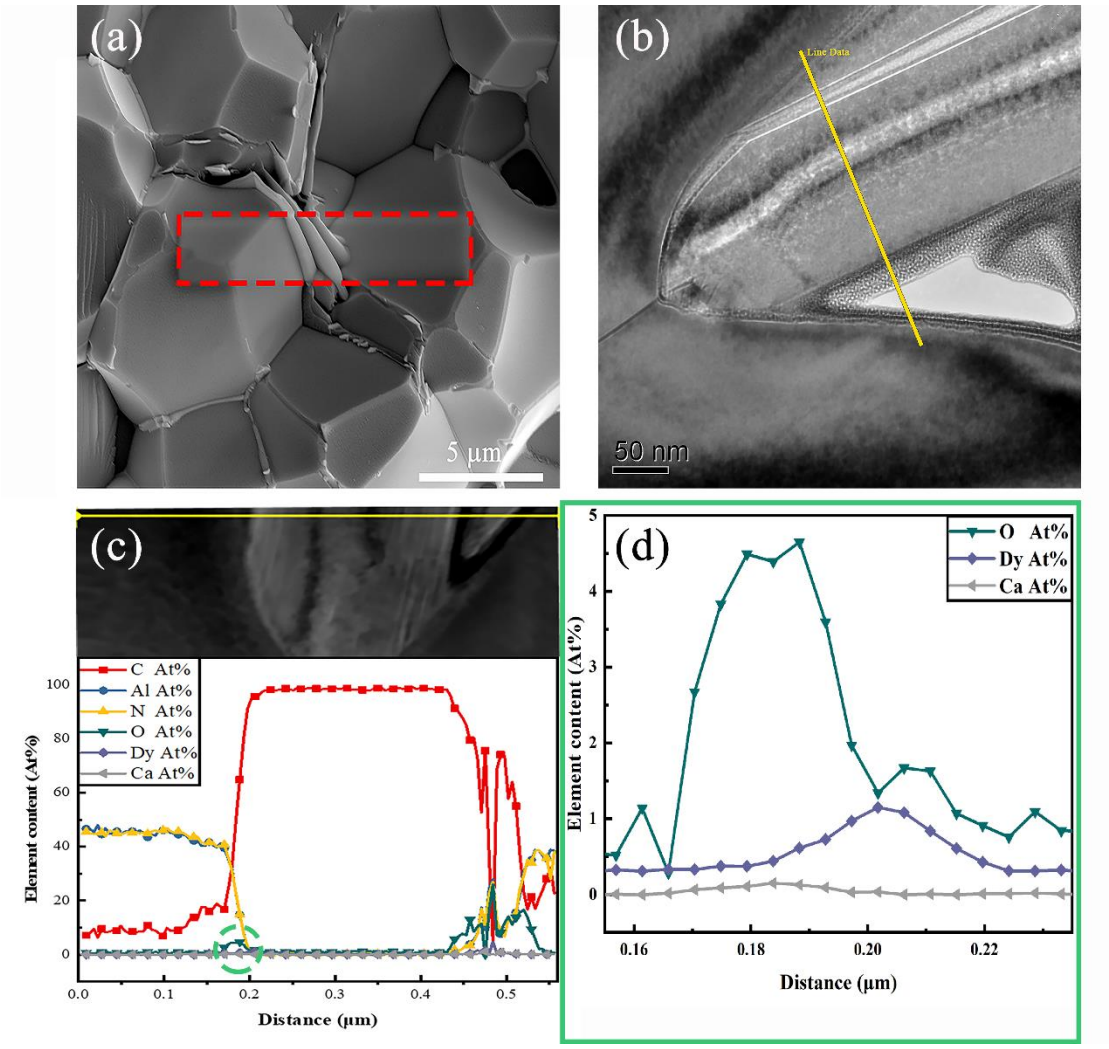

Fig. 6. Element distribution in the grain boundary of AlN ceramic: (a) the SEM of AlN/C grain boundary; (b) the TEM of AlN/Graphite grain boundary; (c) the all element distribution; (d) the special element distribution details at the green area in the (c).

The O enrichment region was closer to the AlN grains, and the Dy enrichment region was more adjacent to the graphite. During the AlN sintering period, the $Al_xDy_yO_{3(x+y)/2}$ was first formed by the reaction between Dy_2O_3 and Al_2O_3. Then $Al_xDy_yO_{3(x+y)/2}$ was reduced by the graphite. The carbothermal reduction reaction reduces the oxygen content around the graphite. Thus, the O and Dy enriched areas have some differences. The nearer it was to graphite, the smaller the content of the O element, which has the existing step concentration in the grain boundary. During the sintering process, oxygen impurities diffused towards the grain boundary and produced a grain boundary phase with Dy_2O_3. The grain boundary phase was finally reduced by graphite at the grain boundary through the carbothermal reduction reaction, cutting down the amounts of oxygen impurities. Therefore, graphite can reduce the oxygen impurities at the grain boundary, purify the lattice and grain boundaries, and improve thermal conductivity.

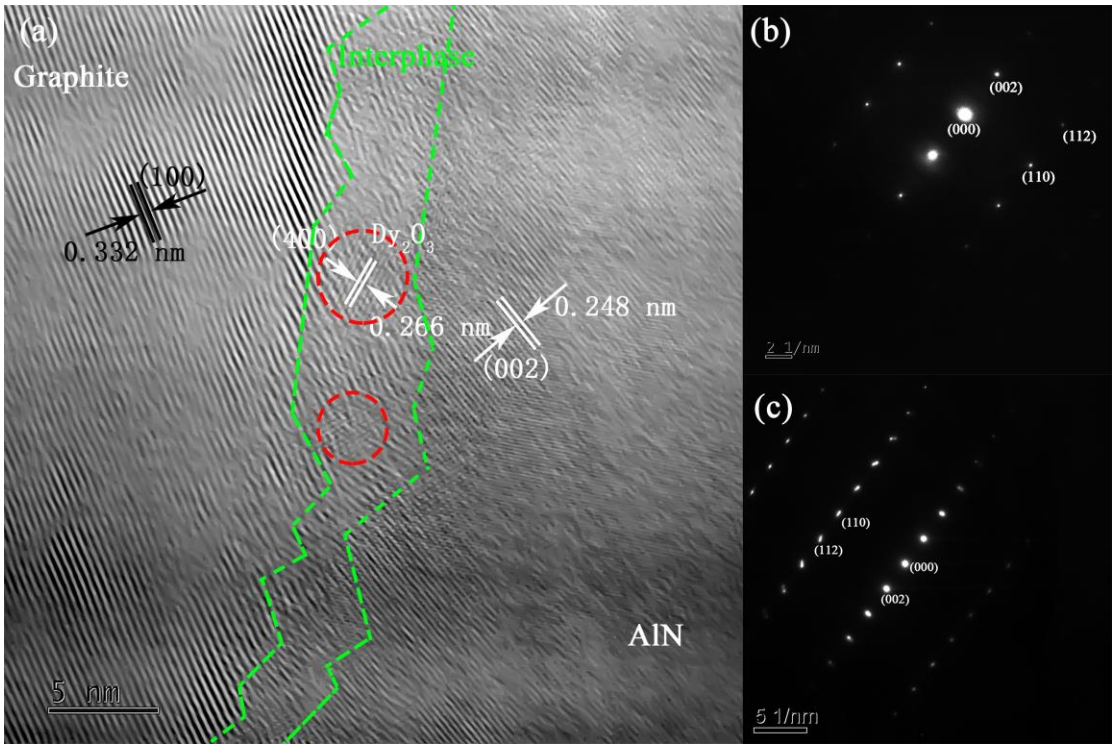

Fig. 7 HRTEM and SAED pattern image of graphite-doped AlN ceramic: (a) HRTEM of grain boundary of AlN/Graphite; (b) SAED pattern image of AlN grain; (c) SAED pattern image of graphite phase.

The microstructure of the AlN with the addition of 1 wt% graphite was observed by TEM. The morphology and structure of grain and grain boundary of AlN ceramics were observed by HRTEM from Fig. 7. A large amount of flake graphite existed between AlN grains, which was further confirmed as the Graphite-2H by the SAED (selected area electron diffraction) pattern, according to Fig. 7c. The structure and crystal lattice of graphite were hexagonal structure and $P6_3mc$ (194), respectively. The standard card PDF corresponding with Graphite-2H is PDF#04-006-5764. The SAED pattern of AlN grain was also observed from Fig. 7b. The structure and crystal lattice of AlN were hexagonal structure and $P6_3mc$ (186), respectively. The standard card PDF corresponding with AlN-Wurtzite is PDF#04-003-5900.

Fig. 7a shows a high-resolution grain boundary image. This area consisted of three parts. The lattice image of the left crystal phase was that of graphite, the interplanar spacing was 0.333 nm, and the direction was along the (100) crystal plane. The right lattice image was AlN phase, the interplanar spacing was 0.248 nm, and the direction was along the (002) crystal plane. There were also some thin amorphous layers between the graphite particles and the AlN grains (Fig. 7a) green dotted line region). A small number of nanocrystals were discovered in this amorphous layer, as shown in the red dotted line region of Fig. 6a. The lattice image of the nanocrystal grains indicated Dy_2O_3, the interplanar spacing was 0.266 nm and 0.229 nm, and the direction was index as the (400) and (332) crystal plane, respectively.

3.4 The mechanism of graphite addition influencing the properties of AlN ceramics

The mechanism that graphite improved the thermal conductivity of AlN ceramic was discussed in Fig. 8. The content of V_{Al}''' has a significant effect on thermal conductivity. The V_{Al}''' was produced by oxygen doping to AlN lattice. With the use of sintering additive in the ceramic preparation process, the oxygen impurities were formed grain boundary phase with sintering additives and hardly diffused into the AlN lattice. However, the grain boundary has a lower thermal conductivity than AlN. The defects might exist in the grain boundary in the process of grain boundary phase production. The grain boundary phase also has a disadvantage to the thermal

conductivity increase of the sample. The grain boundary phase and defects were eliminated using graphite by the carbothermal reduction reaction, as shown in Fig. 8 (b). According to previously researched, the oxygen impurity in the AlN ceramic was discharged as the modality of CO by the cycle of $Dy_2O_3 \rightarrow DAG \rightarrow DAM \rightarrow Dy_2O_3$.

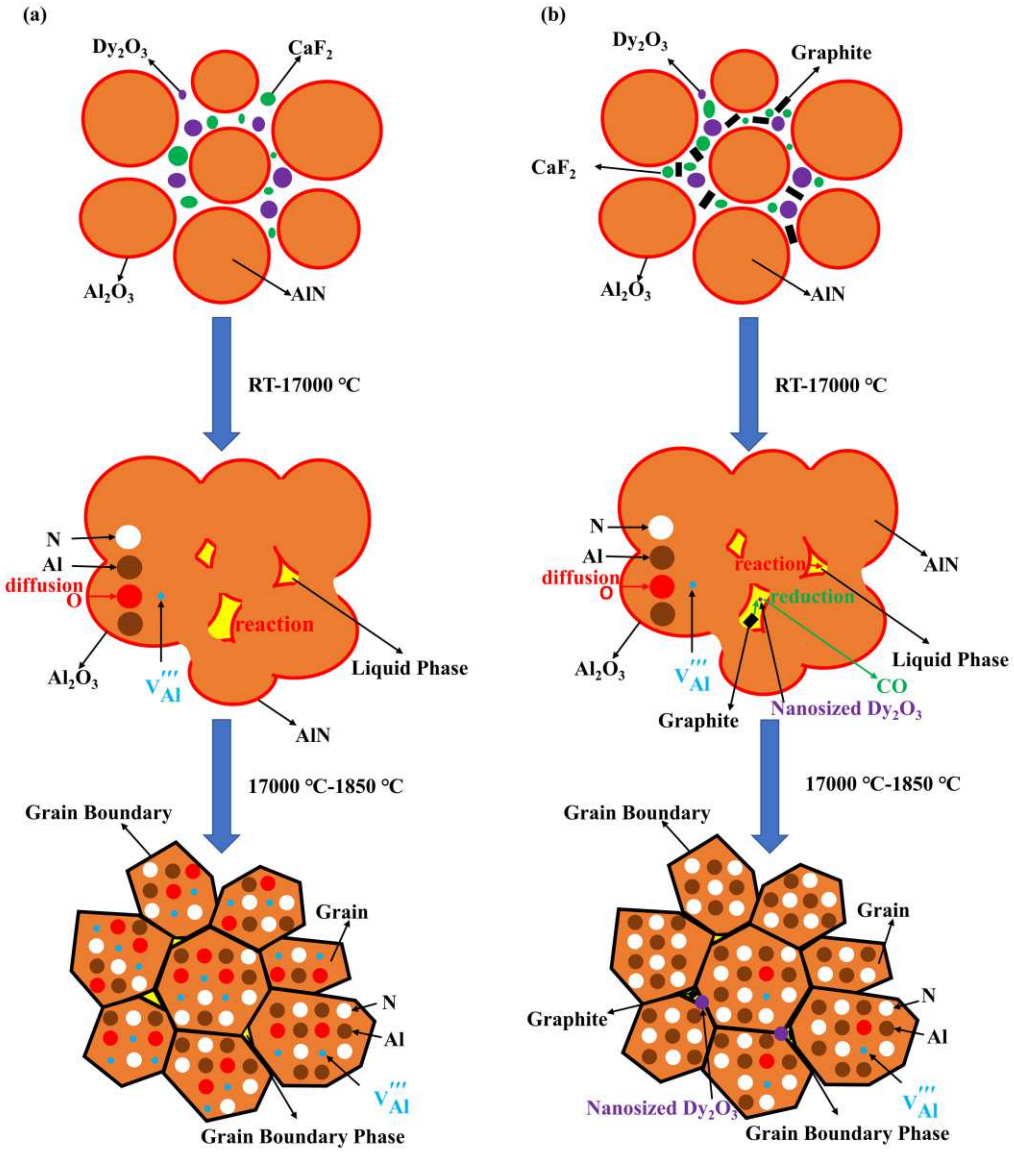

Fig. 8 The schematic diagram of microstructural evolution of AlN ceramics: (a)without graphite and (b) with graphite

3.5 The influence of graphite addition on the impedance spectroscopy of AlN ceramics

The impedance spectroscopy of the AlN sample was measured in a frequency of 0.1 Hz ~ 1 MHz in temperature ranging from 350°C to 650°C (Fig. 9). The different regions of the samples (AlN grains, grain boundaries, and electrodes) were associated with varying RC elements from the impedance spectroscopy. The impedance data of AlN was fitted employing the equivalent circuits containing two parallel R|CPE and an CPE, according to arcs of Z'-Z'' plots and brickwork layer model [36].

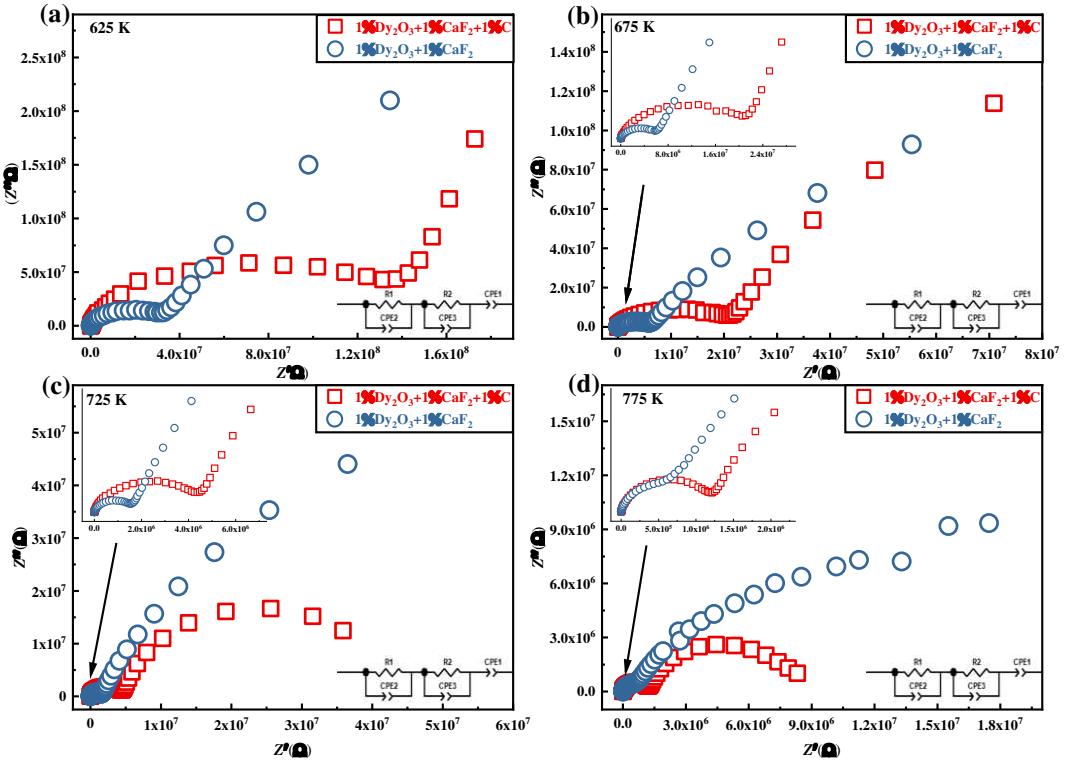

Fig. 9 Complex impedance spectra (Z'–Z'') for monophase AlN ceramics and graphite/AlN multiphase ceramics measured on: (a) 625 K; (b) 675 K; (c) 725 K; (d) 775 K

Fig. 10 shows the conductivity charged with the testing temperature which follows i the Arrhenius equation(equaton 7). And the activation energy (E_a) of the AlN can be calculated from the slope of the curves in Fig. 10.:

$$\sigma = \sigma_0 \exp\left(\frac{-E_a}{k_B T}\right) \tag{7}$$

Where σ_0 is the high-temperature limit of conductivity, E_a is the activation energy, k_B is the Boltzmann constant, T is the absolute temperature.

The grain conductivity (σ_g) and grain boundary conductivity (σ_{gb}) are calculated from equations 8 and 9:

$$\sigma_g = 1/\rho_g = t/R_g \cdot S \tag{8}$$

$$\sigma_{gb} = 1/\rho_{gb} = t/R_{gb} \cdot S \tag{9}$$

Where S and t are the effective electrode area and sample thickness, respectively.

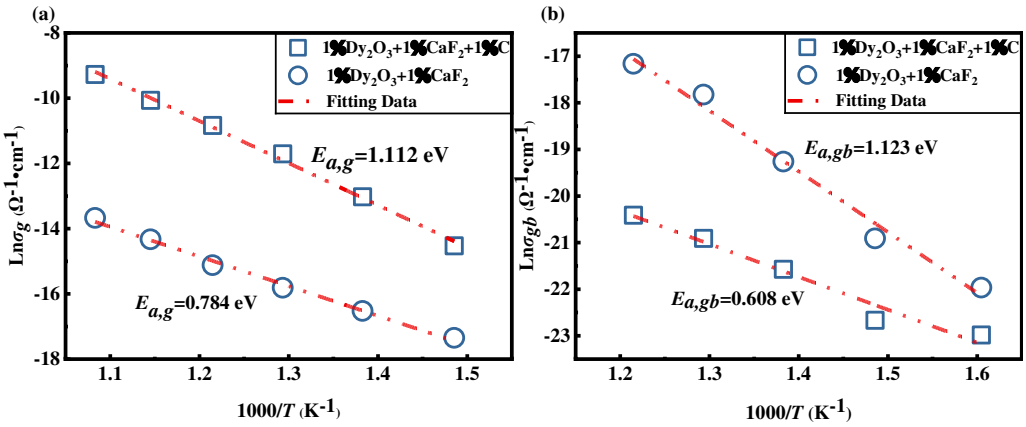

Fig. 10 The Arrhenius plots about temperature and resistivity of the AlN: (a) fitted grain and (b) grain boundary resistivities for the monophase AlN ceramics and graphite/AlN multiphase ceramics

The conductivity mechanism of the AlN grain at high temperature was considered as V_{Al}''' conductance. Oxygen impurities dissolved in the AlN lattice and V_{Al}''' formed at the same time, according to the defect reaction equation (1). The concentration of V_{Al}''' importantly affected the E_a and thermal conductivity of the AlN sample. In the grain, the conductivity behavior of the AlN was closely related to the defects and impurities. In graphite/ AlN ceramics, the E_a value of the graphite/ AlN ceramics is $E_{a,g}$=1.112 eV Which higher than that value ($E_{a,g}$=0.784 eV) of the pure AlN ceramics. Besides, the $E_{a,gb}$ of graphite/ AlN ceramics in grain boundary is 0.608 eV, much smaller than the $E_{a,gb}$=1.123 eV value of monolithic AlN ceramics. The grain

boundary phase is replaced with graphite in the graphite/AlN ceramic as previously discussed by SEM, XRD, and TEM. The grain boundary conductivity of graphite/AlN multiphase ceramic is rapidly improved due to the excellent conductivity properties of graphite. This phenomenon suggests that the graphite materials can effectively reduce the V_{Al}''' and oxygen impurities in AlN grain, purify grain boundary of AlN sample, thus improve the E_a and thermal conductivity of the sample.

4. **Conclusion**

Graphite/AlN multiphase sample doped with 1 wt% Dy_2O_3, 1 wt% CaF_2, and graphite powder was sintered at 1850°C under the flowing N_2 atmosphere. The sample has the optimal relative density (99.98%), thermal conductivity (210 W/m·K) and microstructure with 1 wt% graphite introducing. Oxygen impurities were discharged from the sample in the form of CO by Dy_2O_3→DAG→DAM→Dy_2O_3 periodic changes. The concentration variation of oxygen impurities and aluminum vacancies in AlN ceramics was further proved by E_a value fitting from AC impedance spectroscopy. The graphite can effectively purify the lattice, clean the grain boundary of AlN ceramic, reduce the concentration of oxygen impurities and aluminum vacancies, and improve the thermal conductivity of the samples.

Acknowledgements

This work was supported by the Shanghai Municipal Natural Science Foundation, China (Granted No.19ZR1418500).

Reference

[1] Baskut S, Cinar A, Turan S. Directional properties and microstructures of spark plasma sintered aluminum nitride containing graphene platelets[J]. J Eur Ceram Soc Society 2017, 37(12): 3759-3772.

[2] Li QG, Wang Z, Wu C, et al. Microstructure and mechanical properties of aluminum nitride co-doped with cerium oxide via hot-pressing sintering[J]. J Alloys Compd 2015, 640: 275-279.

[3] Xiong Y, Wang H, Fu ZY. Transient liquid-phase sintering of AlN ceramics with CaF_2 additive[J]. J Eur Ceram Soc Society 2013, 33(11): 2199-2205.

[4] Wang C, Peng C, Wang R, et al. Typical properties and preparation technologies of AlN packaging material[J]. Chin J Nonferrous 2007, 17(11): 1729-1738.

[5] Christensen A, Graham S. Thermal effects in packaging high power light emitting diode arrays[J]. Appl Therm Eng 2009, 29(2-3): 364-371.

[6] Slack GA. Nonmetallic crystals with high thermal conductivity[J]. J Phys Chem Solids 1973, 34(2):321-335.

[7] Slack GA, McNelly TF. Growth of high purity AlN crystals[J]. J Cryst Growth 1976, 34(2): 263-279.

[8] Slack GA, Tanzilli RA, Pohl RO, et al. The intrinsic thermal conductivity of AIN [J]. J Phys Chem Solids 1987, 48(7):641-647.

[9] Lee RR. Development of high thermal conductivity aluminum nitride ceramic[J]. J Am Ceram Soc 1991, 74(9): 2242-2249.

[10] Sakai T, Iwata M. Effect of oxygen on sintering of AlN[J]. J Mater Sci 1977, 12(8):1659-1665.

[11] Sakai T. Effect of the oxygen impurity on the sintering and the thermal conductivity of AlN polycrystal[J]. J Ceram Soc Jpn 1978, 86(992): 174.

[12] Tseng WJ, Tsai CJ. Microporous layer structure in oxidized aluminium nitride polycrystals [J]. J Mater Process Tech 2004, 146(3):289-293.

[13] Abeles B. Lattice Thermal Conductivity of Disordered Semiconductor Alloys at High Temperatures[J]. Phys Rev 1963, 131(5):1906-1911.

[14] Tseng WJ, Tsai CJ. Microporous layer structure in oxidized aluminium nitride polycrystals [J]. J Mater Process Tech 2004, 146(3):289-293.

[15] Callahan DL. Comment on “Diffraction Method Detection of Local Lattice Distortion in AlN Ceramics by Convergent Beam Electron”[J]. J Am Ceram Soc 1996, 79(7):1982-1983.

[16] Qiao L, Zhou H, Chen K, et al. Effects of Li_2O on the low temperature sintering and thermal conductivity of AlN ceramics[J]. J Eur Ceram Soc Society 2003, 23(9): 1517-1524.

[17] Ru Y, Jie Q, Min L, et al. Synthesis of yttrium aluminum garnet (YAG) powder by homogeneous precipitation combined with supercritical carbon dioxide or ethanol fluid drying[J]. J Eur Ceram Soc Society 2008, 28(15): 2903-2914.

[18] Pezzotti G, Nakahira A, Tajika M. Effect of extended annealing cycles on the thermal conductivity of AlN/Y_2O_3 ceramics[J]. J Eur Ceram Soc Society 2000, 20(9):1319-1325.

[19] Xu FM, Zhang ZJ, Shi XL, et al. Effects of adding yttrium nitrate on the mechanical properties of hot-pressed AlN ceramics[J]. J Alloys Compd 2011, 509(35):8688-8691.

[20] Lai G, Nagai Y. Effect of oxygen on sintering of aluminium nitride with Y_2O_3 sintering aid[J]. J Ceram Soc Jpn 1995, 103(1193): 6-10.

[21] Xiong Y, Fu ZY, Wang H, et al. Microstructure and IR transmittance of spark plasma sintering translucent AlN ceramics with CaF_2 additive[J]. Mater Sci Eng B Solid State Mater Adv Techno 2005, 123(1):57-62.

[22] Jackson TB, Virkar AV, More KL, et al. High-thermal-conductivity aluminum nitride ceramics: the effect of thermodynamic, kinetic, and microstructural factors[J]. J Am Ceram Soc 1997, 80(6): 1421-1435.

[23] Fang Z, Liu Y, Wu Y, et al. Microstructure and dielectric dispersion of low-temperature sintered AlN[J]. J Mater Sci letters 2000, 19(2): 95-97.

[24] Kume S, Yasuoka M, Lee SK, et al. Dielectric and thermal properties of AlN ceramics[J]. J Eur Ceram Soc Society 2007, 27(8):2967-2971.

[25] Klein PH, Croft WJ. Thermal Conductivity, Diffusivity, and Expansion of Y_2O_3, $Y_3Al_5O_{12}$, and LaF_3 in the Range 77–300 K[J]. J Appl Phys 1967, 38(4): 1603-1607.

[26] Kurokawa Y, Utsumi K, Takamizawa H. Development and microstructural characterization of high‐thermal‐conductivity aluminum nitride ceramics[J]. J Am Ceram Soc 1988, 71(7): 588-594.

[27] Ivanov SN, Popov PA, Egorov GV, et al. Thermophysical properties of aluminum nitride ceramic[J]. Phys Solid State+ 2002, 206-213(1):699-702.

[28] Buhr H, Müller G. Microstructure and thermal conductivity of AlN(Y_2O_3) ceramics sintered in different atmospheres[J]. J Eur Ceram Soc Society 1993, 12(4):271-277.

[29] Bickermann M, Epelbaum BM, Winnacker A. Characterization of bulk AlN with low oxygen content[J]. J Cryst Growth 2004, 269(2):432-442.

[30] Watari K, Tsugoshi T, Nagaoka T, et al. Microstructure and Thermal Conductivity of AlN Ceramic with Eliminated Grain Boundary Phase[J]. Key Eng Mater 2003, 247:361-364.

[31] Watari K, Tsuzuki A, Torii Y. Effect of rare-earth oxide addition on the thermal conductivity of sintered aluminium nitride[J]. J Mater Sci Letters 1992, 11(22):1508-1510.

[32] Watari K, Nakano H, Urabe K, et al. Thermal conductivity of AlN ceramic with a very low amount of grain boundary phase at 4 to 1000 K[J]. J Mater Res 2002, 17(11):2940-2944.

[33] Kim H, Chae J, Oh Y, et al. Effects of carbothermal reduction on the thermal and electrical conductivities of aluminum nitride ceramics[J]. Ceram Int 2010, 36(7): 2039-2045.

[34] Jiang H, Wang XH, Lei W, et al. Effects of two-step sintering on thermal and mechanical properties of aluminum nitride ceramics by impedance spectroscopy analysis[J]. J Eur Ceram Soc Society 2019, 39(2-3): 249-254.

[35] Wang T, Xie JJ, Dai SH, et al. Influence of Dy_2O_3–CaF_2 Addition on Preparation, Microstructure and Properties of AlN Ceramics[J]. J Chin Ceram Soc 2018,46(06):760-765.

[36] Wang K, Wang C. Aluminum‐vacancy‐related dielectric relaxations in AlN ceramics[J]. J Am Ceram Soc 2018, 101(5): 2009-2016.

Graph Abstract:

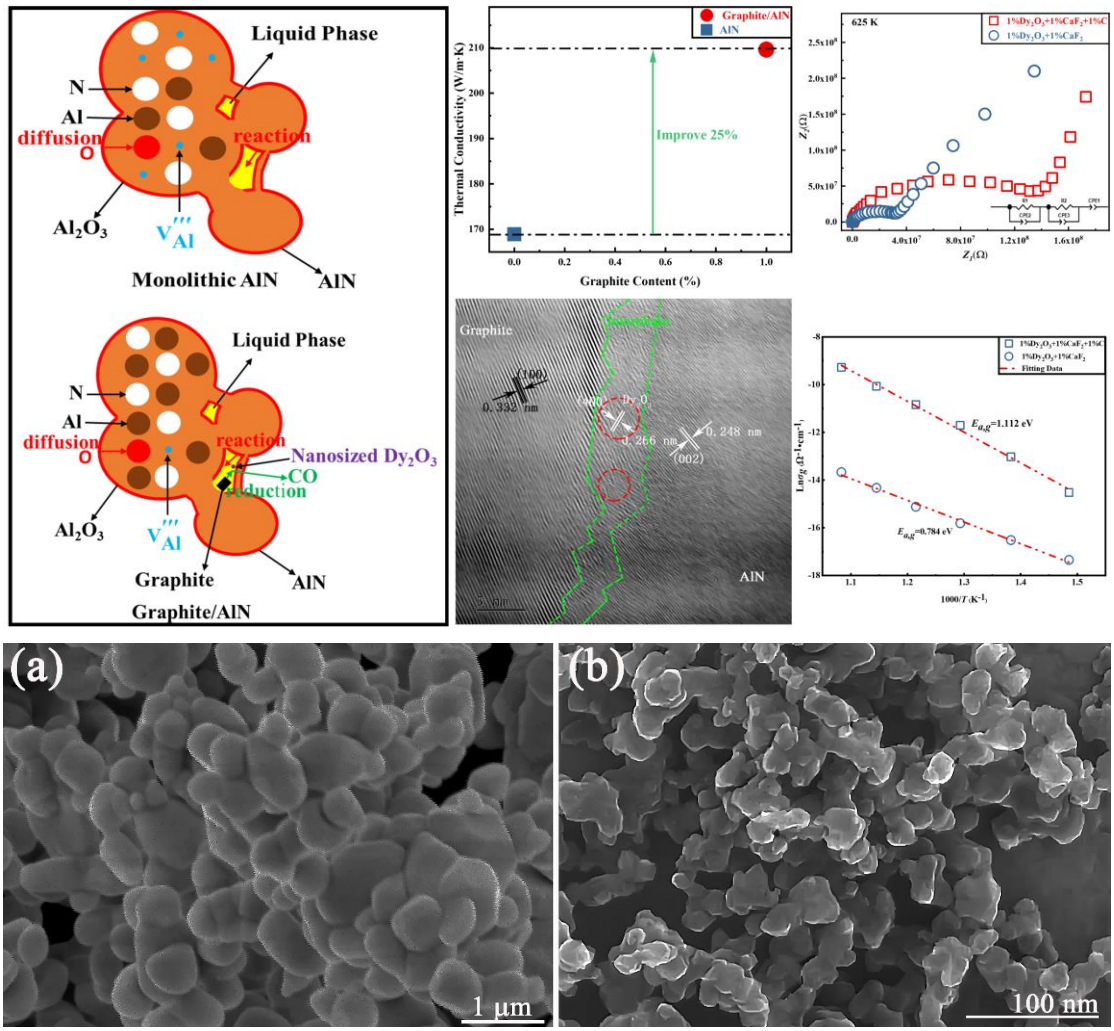

Fig. 1 The SEM micrograph of: (a) AlN powder and (b) grahite powder.

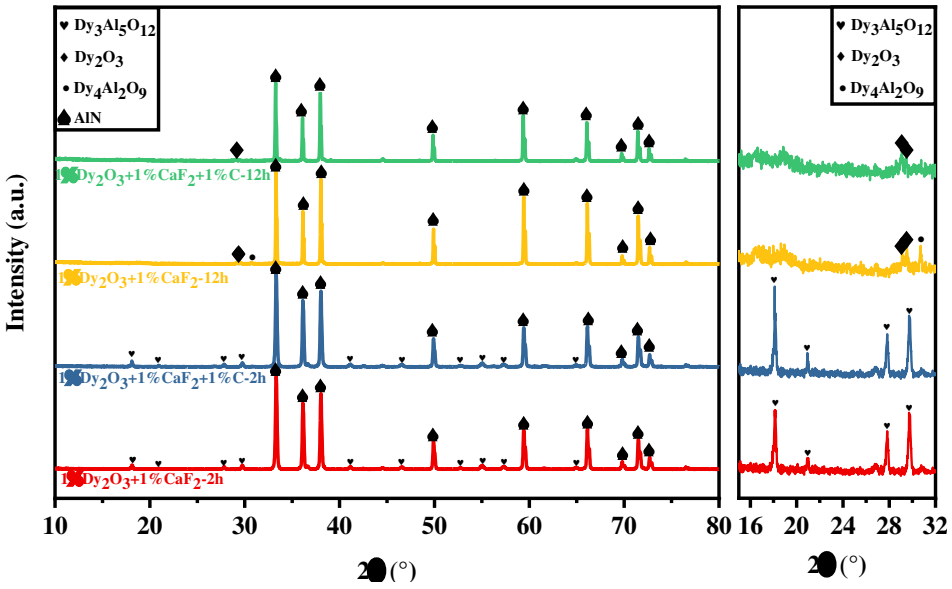

Fig. 2 XRD patterns of Graphite/AlN multpahse ceramics sintered at 1850°C.

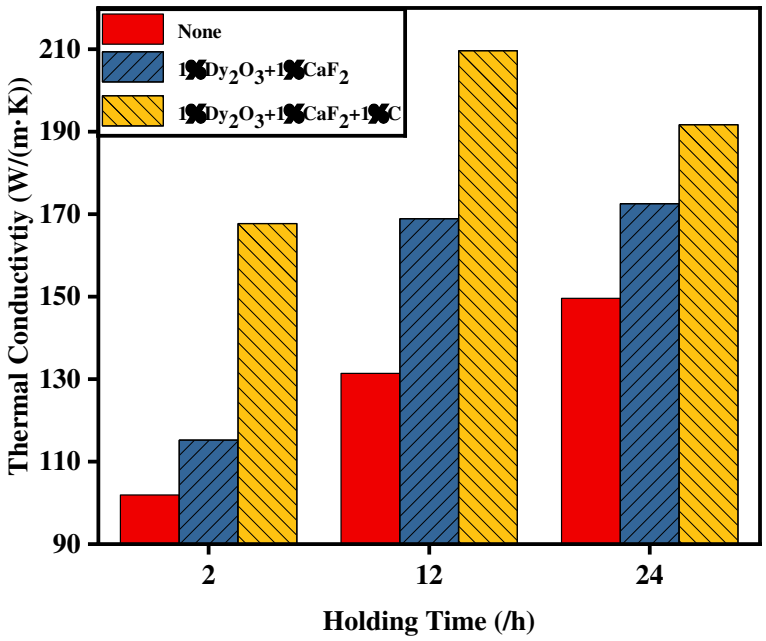

Fig. 3 The dependence of holding times on the thermal conductivity of the AlN sample with 1 wt% graphite sintered at 1850°C.

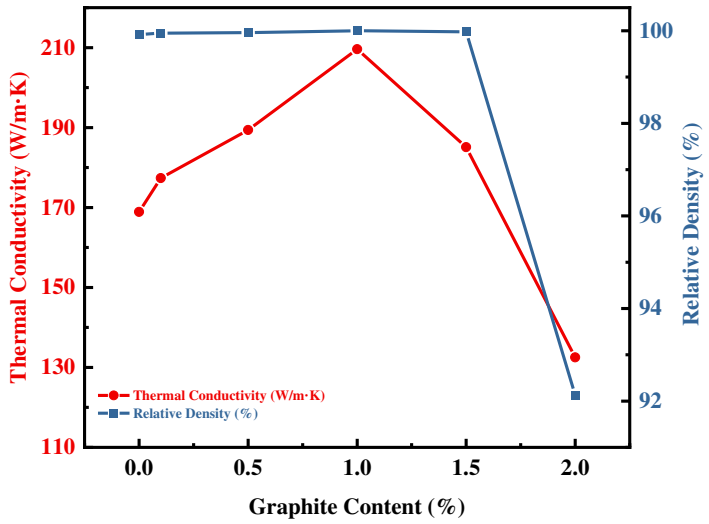

Fig. 4 The influence of graphite on thermal conductivity and relative density of AlN sample sintered at 1850°C for 12 h.

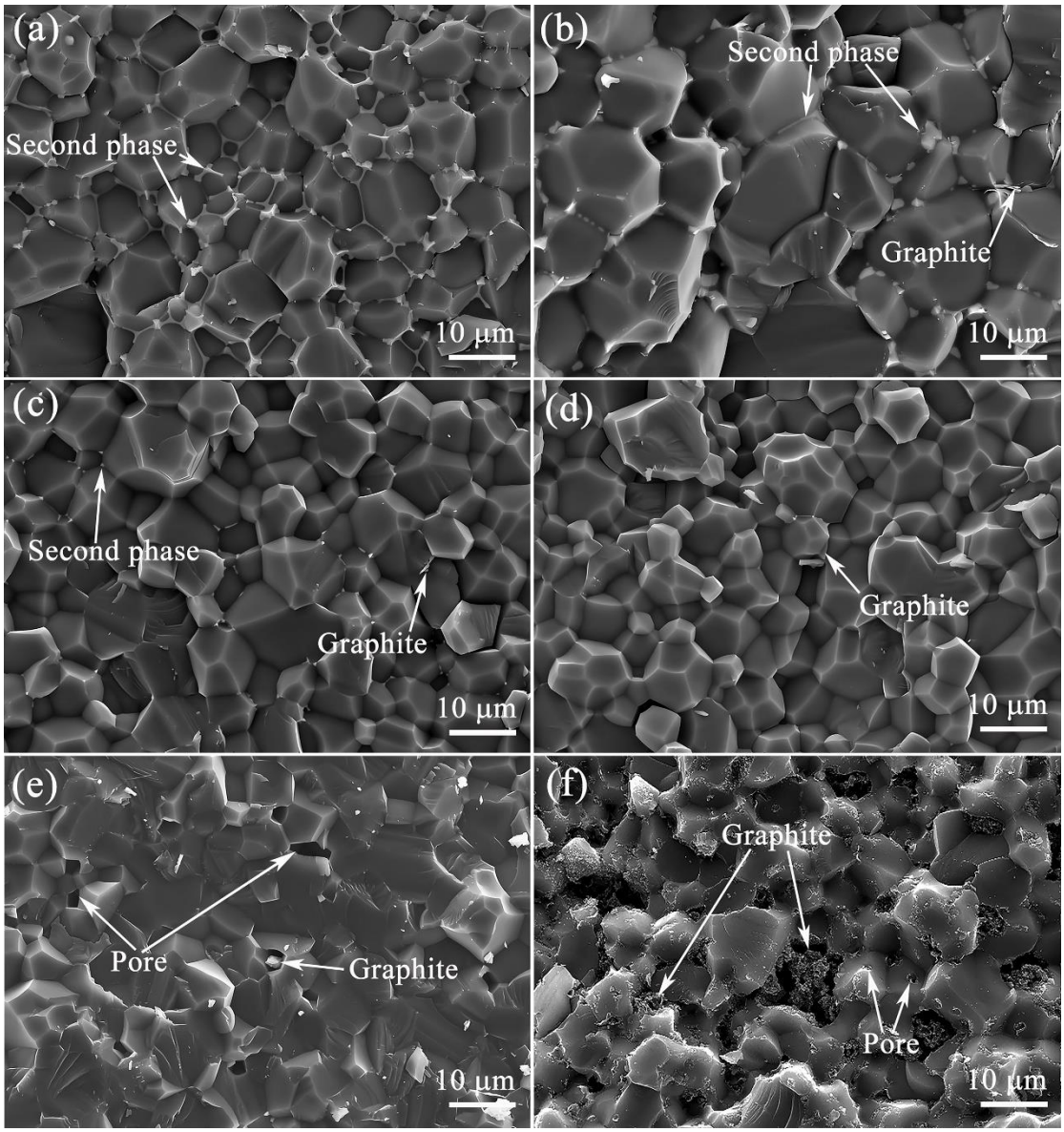

Fig. 5 The microstructure evolution of different graphite content AlN sample sintered at 1850°C for 12 h: (a) C_0; (b) $C_{0.1}$; (c) $C_{0.5}$; (d) C_1; (e) $C_{1.5}$; (f) C_2.

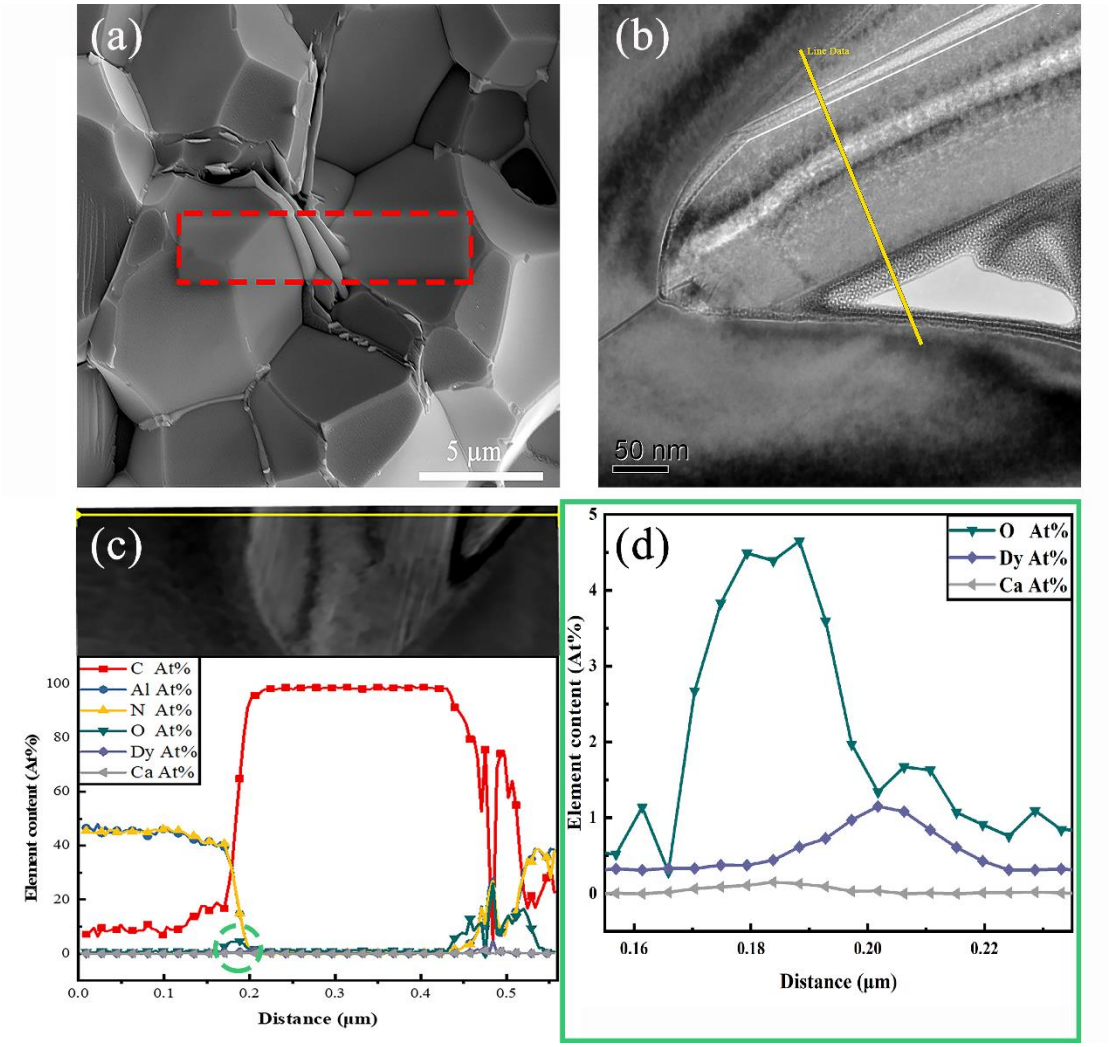

Fig. 6. Element distribution in the grain boundary of AlN ceramic: (a) the SEM of AlN/C grain boundary; (b) the TEM of AlN/C grain boundary; (c) the all element distribution; (d) the special element distribution details at the green area in the (c).

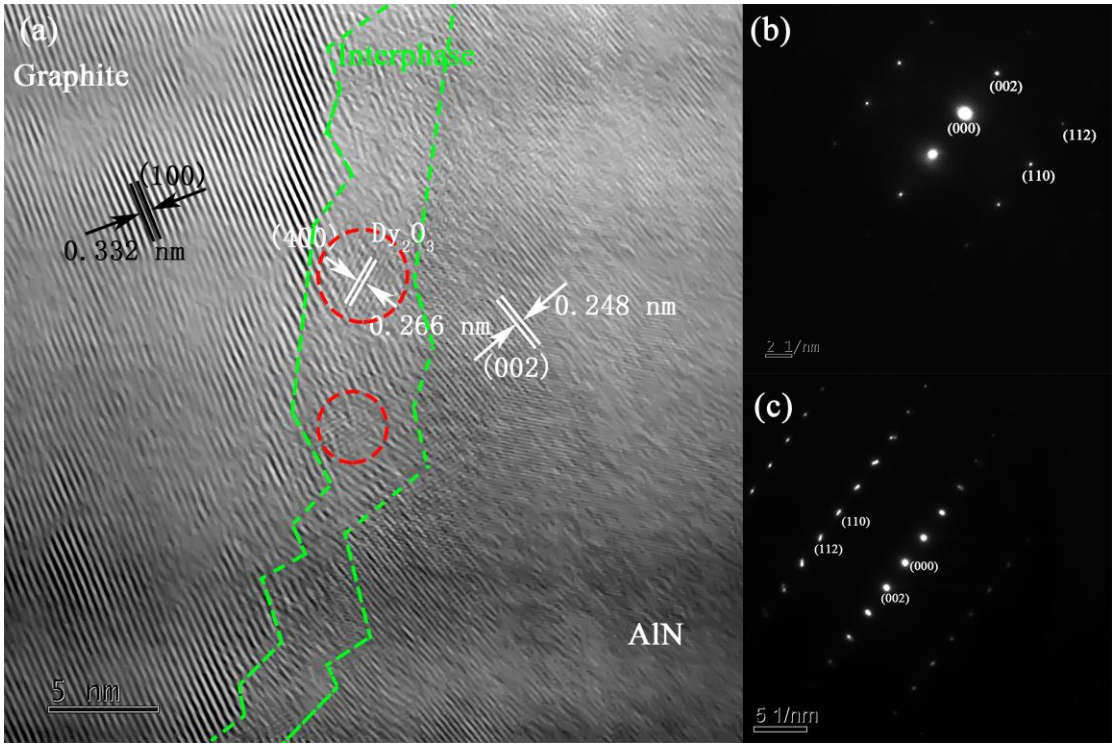

Fig. 7 HRTEM and SAED pattern image of graphite-doped AlN ceramic: (a) HRTEM of grain boundary of AlN/Graphite; (b) SAED pattern image of AlN grain; (c) SAED pattern image of graphite phase.

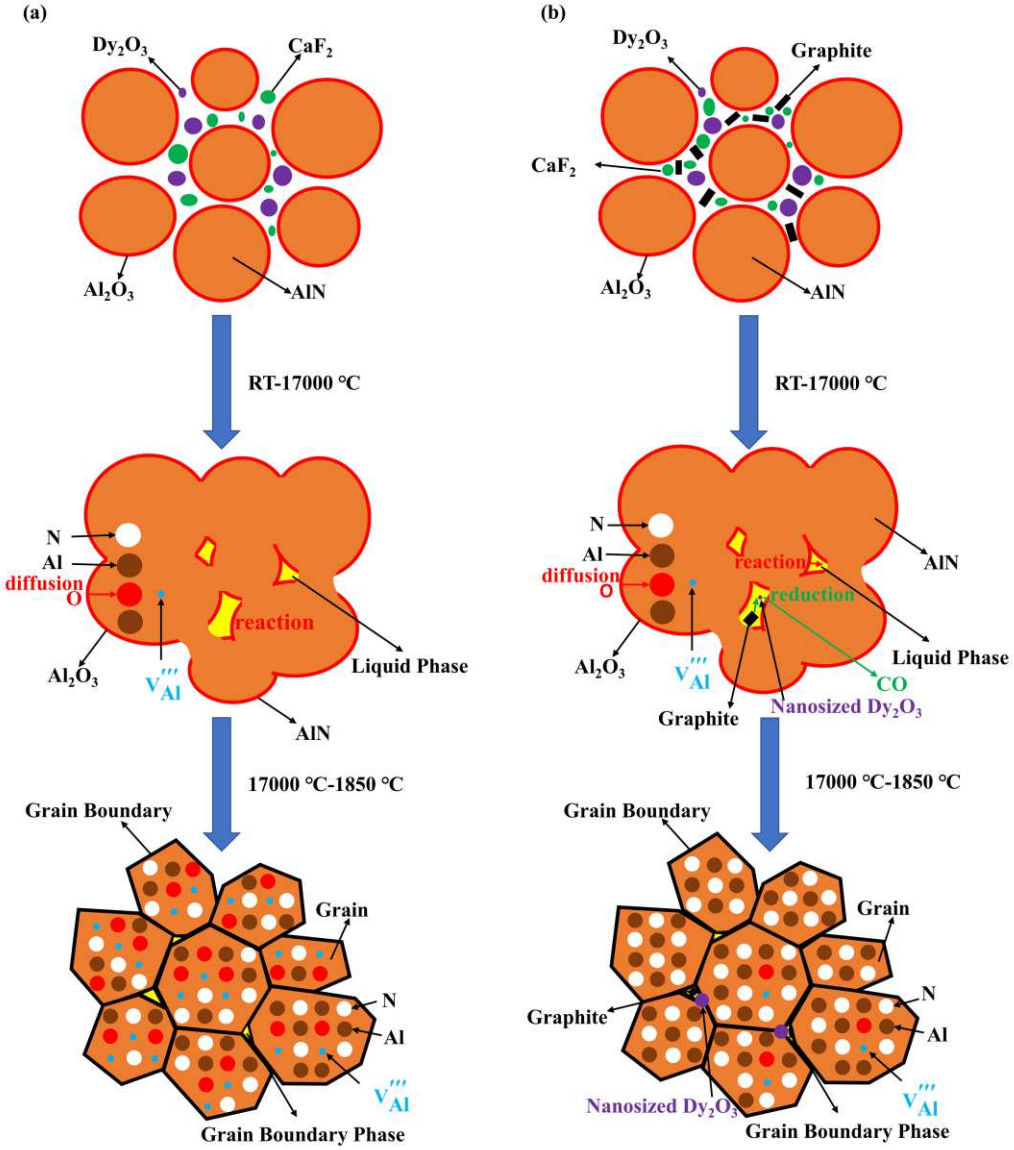

Fig. 8 The schematic diagram of microstructural evolution of AlN ceramics: (a)without graphite and (b) with graphite

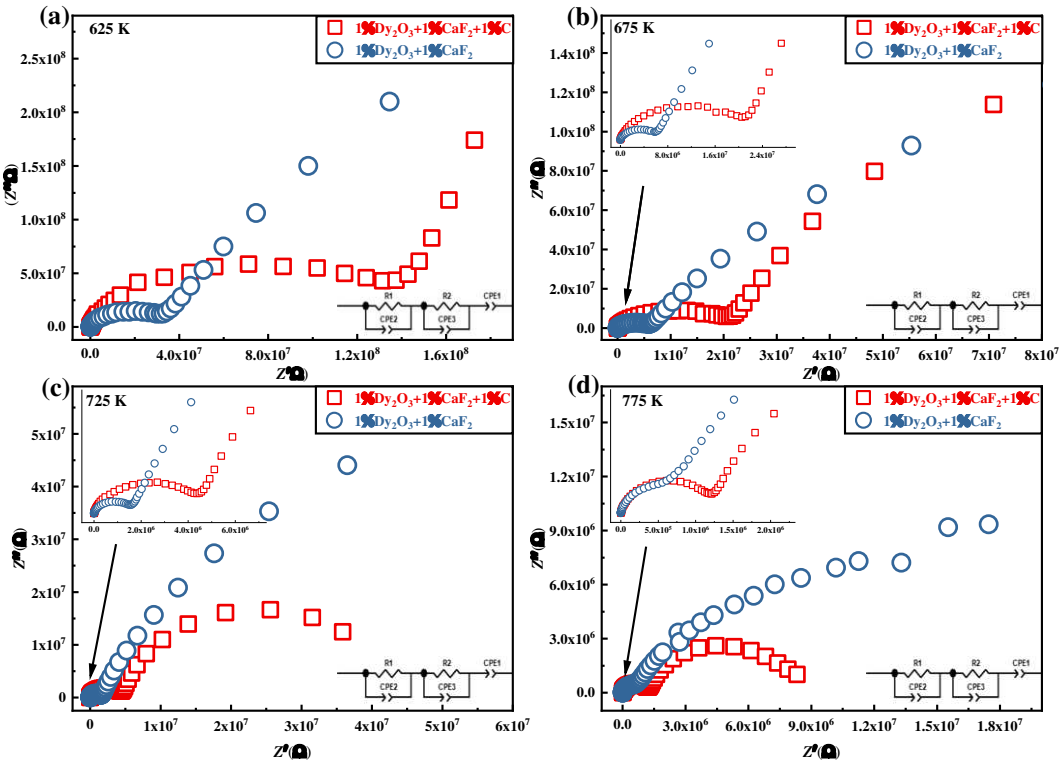

Fig. 9 Complex impedance spectra (Z'–Z'') for monophase AlN ceramics and graphite/AlN multiphase ceramics measured on: (a) 625 K; (b) 675 K; (c) 725 K; (d) 775 K

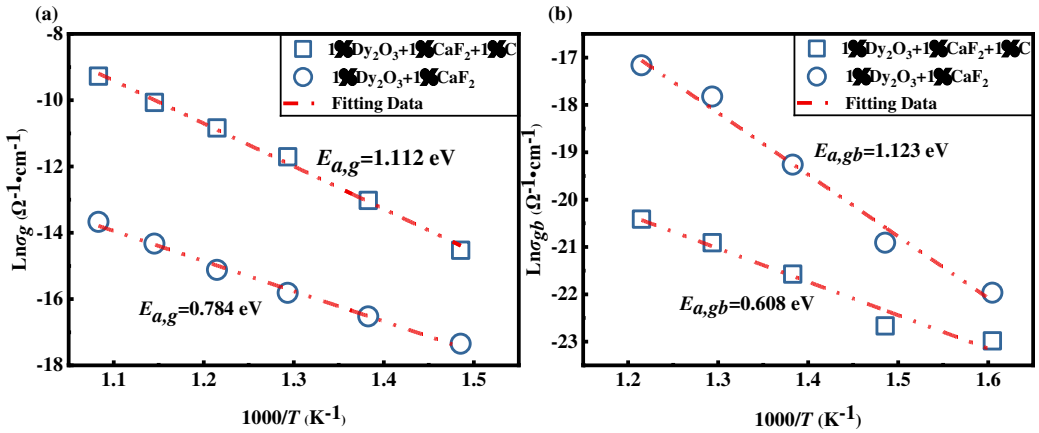

Fig. 10 The Arrhenius plots about temperature and resistivity of the AlN: (a) fitted grain and (b) grain boundary resistivities for the monophase AlN ceramics and graphite/AlN multiphase ceramics

Table 1 Compositions of prepared AlN samples

Symbol	Sample composition (mass%)			
	Dy_2O_3	CaF_2	Grahpite	AlN
C_0	1	1	0	98
$C_{0.1}$	1	1	0.1	97.9
$C_{0.5}$	1	1	0.5	97.5
C_1	1	1	1	97
$C_{1.5}$	1	1	1.5	97.5
C_2	1	1	2	96